Inorganic Chemistry

Article

Synthesis and Characterization of a Mn$_{22}$ Single-Molecule Magnet and a [Mn$_{22}$]$_n$ Single-Chain Magnet

Jonathan T. Brockman,[†] Theocharis C. Stamatatos,[†] Wolfgang Wernsdorfer,[‡] Khalil A. Abboud,[†] and George Christou*,[†]

Department of Chemistry, University of Florida, Gainesville, Florida 32611-7200, and Institut Néel, CNRS/UJF, BP 166, 25 Avenue des Martyrs, 38042 Grenoble, Cedex 9, France

The reactions of [Mn$_{12}$O$_{12}$(O$_2$CEt)$_{16}$(H$_2$O)$_4$] with phenylphosphinic acid (PhHPO$_2$H) in MeCN and MeCN/CH$_2$Cl$_2$ have led to isolation of [Mn$_{22}$O$_{12}$(O$_2$CEt)$_{22}$(O$_3$PPh)$_8$(H$_2$O)$_8$] (**2**) and [Mn$_{22}$O$_{12}$(O$_2$CEt)$_{20}$(O$_3$PPh)$_8$(O$_2$PPhH)$_2$(H$_2$O)$_8$]$_n$ (**3**), respectively, both containing PhPO$_3^{2-}$ groups from in situ oxidation of PhPO$_2^-$. Complex **2** is molecular and consists of two Mn$_9$ subunits linked by four additional Mn atoms. Complex **3** contains almost identical Mn$_{22}$ units as **2**, but they are linked into a one-dimensional chain structure. The Mn$_{22}$ unit in both compounds is mixed-valence Mn$^{III}_{18}$, Mn$^{II}_4$. Solid-state, variable-temperature dc magnetic susceptibility and magnetization measurements were performed on vacuum-dried samples of **2** and **3**, indicating dominant antiferromagnetic interactions. A good fit of low-temperature magnetization data for **2** could not be obtained because of problems associated with low-lying excited states, as expected for a high nuclearity complex containing Mn^{II} atoms. An approximate fit using only data collected in small applied fields indicated an $S = 7$ or 8 ground state for **2**. Solid-state ac susceptibility data established that the true ground state of **2** is $S = 7$ and that the connected Mn$_{22}$ units of **3** are ferromagnetically coupled. Both **2** and **3** displayed weak out-of-phase ac signals indicative of slow magnetization relaxation. Single-crystal magnetization versus applied dc field scans exhibited hysteresis loops for both compounds, establishing them as new single-molecule and single-chain magnets, respectively. Complex **2** also showed steps in its hysteresis loops characteristic of quantum tunneling of magnetization, the highest nuclearity molecule to show such QTM steps. Arrhenius plots constructed from dc magnetization versus time decay plots gave effective barriers to magnetization relaxation (U_{eff}) of 6 and 11 cm^{-1} for **2** and **3**, respectively.

Introduction

The preparation of new polynuclear Mn complexes has blossomed over the past two decades. The possibility of discovering new clusters simply for their structural aesthetics is motivation in itself, but a more practical and major objective is the search for new examples of single-molecule magnets (SMMs).[1–3] SMMs are molecular species that can function as nanoscale magnets as a result of their intrinsic properties, rather than as a result of interunit interactions and long-range ordering, as would be found in traditional magnetic materials (metals, metal oxides, etc.). Thus, each SMM molecule is a single-domain magnetic particle, and this arises from the combination of a large ground-state spin (S) and an Ising (easy-axis) magnetoanisotropy (negative zero-field splitting parameter, D), which results in a barrier to magnetization relaxation whose upper limit is given by $S^2|D|$. There are several families of homometallic and heterometallic SMMs now known, and new ones become available as workers around the world seek to extend this phenomenon as far as possible.

(1) (a) Christou, G.; Gatteschi, D.; Hendrickson, D. N.; Sessoli, R. *MRS Bull.* **2000**, *25*, 66 and references cited therein. (b) Aromi, G.; Brechin, E. K. *Struct. Bonding* **2006**, *122*, 1. (c) Bircher, R.; Chaboussant, G.; Dobe, C.; Güdel, H. U.; Oshsenbein, S. T.; Sieber, A.; Waldmann, O *Adv. Funct. Mater.* **2006**, *16*, 209.
(2) (a) Sessoli, R.; Gatteschi, D.; Caneschi, A.; Novak, M. A. *Nature* **1993**, *365*, 141. (b) Sessoli, R.; Ysai, H.-L.; Schake, A. R.; Wang, S.; Vincent, J. B.; Folting, K.; Gatteschi, D.; Christou, G.; Hendrickson, D. N. *J. Am. Chem. Soc.* **1993**, *115*, 1804.
(3) (a) Aromi, G.; Aubin, S. M. J.; Bolcar, M. A.; Christou, G.; Eppley, H. J.; Folting, K.; Hendrickson, D. N.; Huffman, J. C.; Squire, R. C.; Tsai, H.-L.; Wang, S.; Wemple, M. W. *Polyhedron* **1998**, *17*, 3005. (b) Christou, G. *Polyhedron* **2005**, *24*, 2065.

The preparation of new Mn SMMs has often employed one of the following strategies: (i) ligand substitution of some or all of the peripheral ligands in preformed Mn_{12} compounds with retention of the basic core structure,[4,5] (ii) structural transformation of a Mn_{12} core to a new structural type by reaction with some suitably chosen chelate or other reagent,[6] and (iii) direct reaction of a simple starting material such as $Mn(O_2CMe)_2 \cdot 4H_2O$ with the appropriate ligands.[3] Of the SMMs known to date, the $[Mn_{12}O_{12}(O_2CR)_{16}(H_2O)_4]$ (Mn_{12}) family with $S = 10$ is the most thoroughly studied, and it has also proven a rich source of new complexes by both routes i and ii. For example, a number of Mn_{12} derivatives have been prepared by ligand substitution reactions (i) with carboxylate and even non-carboxylate sources, allowing among other things for the solubility and redox properties to be tuned.[4,5] Mn_{12} compounds have also proven to be good starting materials for preparing other high-nuclearity Mn_x complexes by route ii including $[Mn_{21}O_{24}(OMe)_8(O_2CCH_2Bu^t)_{16}(H_2O)_{10}]$,[6b] $[Mn_{30}O_{24}(OH)_8(O_2CCH_2Bu^t)_{32}(H_2O)_2(MeNO_2)_4]$,[6a,e] and the largest Mn-carboxylate cluster obtained to date, $[Mn_{84}O_{72}(O_2CMe)_{78}(OMe)_{24}(MeOH)_{12}(H_2O)_{42}(OH)_6]$,[6f] all of which have been new SMMs.

The present results have arisen from continuing our interest in the reactions of Mn_{12} with P-, S-, and Se-based acids. Published progress has included the site-selective replacement of some of the carboxylate groups of $[Mn_{12}O_{12}(O_2CR)_{16}(H_2O)_4]$ with nitrate, diphenylphosphinate, and benzenesulfonate anions to give products such as $[Mn_{12}O_{12}(O_2CCH_2Bu^t)_{12}(NO_3)_4(H_2O)_4]$,[4e] $[Mn_{12}O_{12}(O_2CMe)_8(O_2PPh_2)_8(H_2O)_4]$,[4d,7] and $[Mn_{12}O_{12}(O_2CMe)_8(O_3SPh)_8(H_2O)_4]$,[4f,8] respectively. In addition, other groups have reported the replacement of four carboxylate groups with diphenylphosphates to give $[Mn_{12}O_{12}(O_2CPh)_{12}(O_2P(OPh)_2)_4(H_2O)_4]$.[9] In all of these cases, the Mn_{12} core has remained essentially the same. Exceptions have included the product obtained with benzeneseleninic acid ($PhSeO_2H$), which reacted with $[Mn_{12}O_{12}(O_2CMe)_{16}(H_2O)_4]$ to give a new structural type, $[Mn_7O_8(O_2CMe)(O_2SePh)_8(H_2O)]$.[10] When we recently decided to extend our studies with Ph_2PO_2H to the corresponding mono-phenyl derivative, phenylphosphinic acid ($PhHPO_2H$), it was hoped that the smaller bulk of $PhHPO_2^-$ relative to $Ph_2PO_2^-$ might allow complete substitution of the Mn_{12} carboxylate groups, rather than only half as in $[Mn_{12}O_{12}(O_2CMe)_8(O_2PPh_2)_8(H_2O)_4]$. Thus, we had intended this as another example of synthetic route i but instead have found that the greater sensitivity of the P−H bond in $PhHPO_2^-$ to oxidation has led to another example of reaction ii, that is, the isolated product contains a new Mn_x core containing phenylphosphonate groups, $PhPO_3^{2-}$. We herein describe these results, the syntheses, structures, and magnetic properties of compounds containing the mixed valence $[Mn_{18}^{3+}-Mn_4^{2+}O_{12}]^{38+}$ core.

Experimental Section

Syntheses. All manipulations were performed under aerobic conditions using materials as received. $[Mn_{12}O_{12}(O_2CEt)_{16}(H_2O)_4]$ (**1**) was prepared as previously described.[4a]

$[Mn_{22}O_{12}(O_2CEt)_{22}(O_3PPh)_8(H_2O)_8]$ (2). $PhHPO_2H$ (0.54 g, 3.83 mmol) was added to a solution of complex **1** (1.00 g, 0.48 mmol) in MeCN (30 mL). The mixture was stirred overnight, and the resulting brown slurry was filtered. The filtrate was allowed to concentrate by slow evaporation until precipitation of a brown powder was observed. The powder was removed by filtration, and the filtrate was maintained very slowly evaporating at ambient temperature for several weeks until black crystals of **2**·6MeCN·2CH₂Cl₂ had grown. The yields were small (2−5%) but reproducible, and the crystals were suitable for X-ray crystallography. Material dried under vacuum overnight for analysis appeared to lose bound waters and analyzed as $[Mn_{22}O_{12}(O_2CEt)_{22}(O_3PPh)_8(H_2O)_2]$. Anal. Calcd: C, 31.90; H, 3.62; N, 0.00%. Found: C, 31.81; H, 3.61; N, 0.01%. Selected IR data (cm⁻¹): 3420 (br), 3057

(4) (a) Eppley, H. J.; Tsai, H.-L.; de Vries, N.; Folting, K.; Christou, G.; Hendrickson, D. N. *J. Am. Chem. Soc.* **1995**, *117*, 301. (b) Aubin, S. M. J.; Spagna, S.; Eppley, H. J.; Sager, R. E.; Christou, G.; Hendrickson, D. N. *Chem. Commun.* **1998**, 803. (c) Soler, M.; Chandra, S. K.; Ruiz, D.; Davidson, E. R.; Hendrickson, D. N.; Christou, G. *Chem. Commun.* **2000**, 2417. (d) Boskovic, C.; Pink, M.; Huffman, J. C.; Hendrickson, D. N.; Christou, G. *J. Am. Chem. Soc.* **2001**, *123*, 9914. (e) Artus, P.; Boskovic, C.; Yoo, J.; Streib, W. E.; Brunel, L.-C.; Hendrickson, D. N.; Christou, G. *Inorg. Chem.* **2001**, *40*, 4199. (f) Chakov, N. E.; Wernsdorfer, W.; Abboud, K. A.; Hendrickson, D. N.; Christou, G. *Dalton Trans.* **2003**, 2243. (g) Morello, A.; Bakharev, O. N.; Brom, H. B.; de Jongh, L. J. *Polyhedron* **2003**, *22*, 1745. (h) Bian, G.-Q.; Kuroda-Sowa, T.; Konaka, H.; Hatano, M.; Maekawa, M.; Munakata, M.; Miyasaka, H.; Yamashita, M. *Inorg. Chem.* **2004**, *43*, 4790. (i) Ruiz, D.; Sun, Z.; Albela, B.; Folting, K.; Ribas, J.; Christou, G.; Hendrickson, D. N. *Angew. Chem., Int. Ed. Engl.* **1998**, *37*, 300. (j) Aubin, S. M. J.; Sun, Z.; Guzei, I. A.; Rheingold, A. L.; Christou, G.; Hendrickson, D. N. *J. Chem. Soc., Chem. Commun.* **1997**, 2239. (k) Chakov, N. E.; Lawrence, J.; Harter, A. G.; Hill, S. O.; Dalal, N. S.; Wernsdorfer, W.; Abboud, K. A.; Christou, G. *J. Am. Chem. Soc.* **2006**, *128*, 6975. (l) Soler, M.; Artus, P.; Folting, K.; Huffman, J. C.; Hendrickson, D. N.; Christou, G. *Inorg. Chem.* **2001**, *40*, 4902.

(5) (a) Chakov, N. E.; Soler, M.; Wernsdorfer, W.; Abboud, K. A.; Christou, G. *Inorg. Chem.* **2005**, *44*, 5304. (b) Aubin, S. M. J.; Sun, Z.; Pardi, L.; Krzystek, J.; Folting, K.; Brunel, L.-C.; Rheingold, A. L.; Christou, G.; Hendrickson, D. N. *Inorg. Chem.* **1999**, *38*, 5329. (c) Soler, M.; Wernsdorfer, W.; Abboud, K. A.; Huffman, J. C.; Davidson, E. R.; Hendrickson, D. N.; Christou, G. *J. Am. Chem. Soc.* **2003**, *125*, 3576. (d) Soler, M.; Wernsdorfer, W.; Abboud, K. A.; Hendrickson, D. N.; Christou, G. *Polyhedron* **2003**, *22*, 1777. (e) Soler, M.; Chandra, S. K.; Ruiz, D.; Davidson, E. R.; Hendrickson, D. N.; Christou, G. *Chem. Commun.* **2000**, 2417. (f) Soler, M.; Chandra, S. K.; Ruiz, D.; Huffman, J. C.; Hendrickson, D. N.; Christou, G. *Polyhedron* **2001**, *20*, 1279.

(6) (a) Soler, M.; Rumberger, E.; Folting, K.; Hendrickson, D. N.; Christou, G. *Polyhedron* **2001**, *20*, 1365. (b) Brockman, J. T.; Huffman, J. C.; Christou, G. *Angew. Chem., Int. Ed.* **2002**, *41*, 2506. (c) Brechin, E. K.; Boskovic, C.; Wernsdorfer, W.; Yoo, J.; Yamaguchi, A.; Sañudo, E. C.; Concolino, T. R.; Rheingold, A. L.; Ishimoto, H.; Hendrickson, D. N.; Christou, G. *J. Am. Chem. Soc.* **2002**, *124*, 9710. (d) Boskovic, C.; Huffman, J. C.; Christou, G. *Chem. Commun.* **2002**, 2502. (e) Soler, M.; Wernsdorfer, W.; Folting, K.; Pink, M.; Christou, G. *J. Am. Chem. Soc.* **2004**, *126*, 2156. (f) Tasiopoulos, A. J.; Vinslava, A.; Wernsdorfer, W.; Abboud, K. A.; Christou, G. *Angew. Chem., Int. Ed.* **2004**, *43*, 2117. (g) Brechin, E. K.; Sanudo, E. C.; Wernsdorfer, W.; Boskovic, C.; Yoo, J.; Hendrickson, D. N.; Yamaguchi, A.; Ishimoto, H.; Concolino, T. E.; Rheingold, A. L.; Christou, G. *Inorg. Chem.* **2005**, *44*, 502.

(7) Brockman, J. T.; Abboud, K. A.; Hendrickson, D. N.; Christou, G. *Polyhedron* **2003**, *22*, 1765.

(8) Chakov, N. E.; Abboud, K. A.; Zakharov, L. N.; Rheingold, A. L.; Hendrickson, D. N.; Christou, G. *Polyhedron* **2003**, *22*, 1759.

(9) Kuroda-Sowa, T.; Fukuda, S.; Miyoshi, S.; Maekawa, M.; Munakata, M.; Miyasaka, H.; Yamashita, M. *Chem. Lett.* **2002**, *31*, 682.

(10) Chakov, N. E.; Wernsdorfer, W.; Abboud, K. A.; Christou, G. *Inorg. Chem.* **2004**, *43*, 5919.

(w), 2976 (m), 2940 (m), 2361 (w), 1560 (vs), 1533 (vs), 1466 (s), 1428 (vs), 1374 (w), 1302 (s), 1243 (w), 1141 (vs), 1086 (m), 1041 (s), 988 (s), 928 (s), 811 (w), 750 (m), 721 (m), 695 (s), 655 (s), 613 (s), 555 (vs).

[Mn$_{22}$O$_{12}$(O$_2$CEt)$_{20}$(O$_3$PPh)$_8$(O$_2$PPhH)$_2$(H$_2$O)$_8$]$_n$ (3). PhHPO$_2$H (0.54 g, 3.83 mmol) was added to a solution of complex **1** (1.00 g, 0.48 mmol) in MeCN/CH$_2$Cl$_2$ (15 mL/15 mL). The mixture was stirred overnight, and the resulting brown slurry was filtered. The filtrate was allowed to concentrate by slow evaporation until precipitation of a brown powder was observed. The mixture was refiltered again, and the filtrate was allowed to slowly concentrate by evaporation over three weeks, during which time dark brown/black crystals of **3·7MeCN** were obtained in 35% yield. The crystals were suitable for X-ray crystallography. Selected IR data (cm^{-1}): 3420 (br), 3057 (w), 2976 (m), 2940 (m), 2361 (w), 1560 (vs), 1533 (vs), 1466 (s), 1428 (vs), 1374 (w), 1302 (s), 1243 (w), 1141 (vs), 1086 (m), 1041 (s), 988 (s), 928 (s), 811 (w), 750 (m), 721 (m), 695 (s), 655 (s), 613 (s), 555 (vs).

X-Ray Crystallography. Data were collected on a Siemens SMART PLATFORM equipped with a CCD area detector and a graphite monochromator using Mo Kα radiation ($\lambda = 0.71073$ Å). Cell parameters were refined using up to 8192 reflections. A full sphere of data (1381 frames) was collected using the ω-scan method (0.3° frame width). The first 50 frames were remeasured at the end of data collection to monitor instrument and crystal stability (maximum correction on I was <1%). Absorption corrections by integration were applied based on measured indexed crystal faces.

The structure of **2·6MeCN·2CH$_2$Cl$_2$** was solved by direct methods in *SHELXTL6*[11] and refined on F^2 using full-matrix least-squares methods. The non-H atoms were treated anisotropically, whereas the hydrogen atoms were introduced in calculated, ideal positions and refined as riding on their respective carbon atoms. A total of 1031 parameters were refined in the final cycle of refinement using 10 510 reflections with $I > 2\sigma(I)$ to yield R1 and wR2 values of 4.85 and 13.66%, respectively.

The structure of **3·7MeCN** was solved by direct methods in *SHELXTL6*,[11] and refined on F^2 using full-matrix least-squares methods. The non-hydrogen atoms were treated anisotropically, whereas the hydrogen atoms were introduced in calculated, ideal positions and refined as riding on their respective carbon atoms. The asymmetric unit consists of one-half of the Mn$_{22}$ cluster and 3.5 MeCN molecules of crystallization. In addition to disorder of the Me groups in several of the EtCO$_2^-$ ligands, there is a PhHPO$_2^-$/EtCO$_2^-$ disorder with a ratio of 3:1. A total of 1170 parameters were refined in the final cycle of refinement using 21 121 reflections with $I > 2\sigma(I)$ to yield R1 and wR2 values of 4.51 and 9.72%, respectively.

Unit cell data and structure refinement details for the two compounds are listed in Table 1.

Other Studies. Infrared spectra in the 400−4000 cm^{-1} range were recorded in the solid state (KBr disks) on a Nicolet NEXUS 670 FTIR spectrophotometer. Elemental analyses (C, H, N) were performed by the in-house facilities of the Department of Chemistry, University of Florida. Variable-temperature DC and AC magnetic susceptibility studies were carried out at the University of Florida on powdered microcrystalline samples in the 1.8−300 K range with a Quantum Design MPMS-XL SQUID magnetometer equipped with a 7 T magnet. Pascal's constants were used to estimate the diamagnetic correction for each complex, which was subtracted from the experimental susceptibility to give the molar magnetic susceptibility (χ_M). Samples for DC studies were embedded in solid

(11) *SHELXTL6*; Bruker-AXS: Madison, WI, 2000.

Table 1. Crystallographic Data for Complexes **2·6MeCN·2CH$_2$Cl$_2$** and **3·7MeCN**

	2	3
formula^a	C$_{128}$H$_{188}$Cl$_4$Mn$_{22}$N$_6$O$_{88}$P$_8$	C$_{132.5}$H$_{187}$Mn$_{22}$N$_7$O$_{88}$P$_{9.5}$
fw, g/mol	4817.08	4788.79
cryst syst	triclinic	monoclinic
space group	P$\bar{1}$	P2$_1$/n
a, Å	15.100(3)	14.9141(8)
b, Å	16.311(3)	21.7205(12)
c, Å	23.866(4)	28.9712(16)
α, deg	101.992(2)	90
β, deg	106.520(2)	94.272(1)
γ, deg	94.217(2)	90
V, Å^3	5457.1(2)	9358.9(9)
Z	1	2
ρ_{calcd}, g cm^{-3}	1.466	1.699
cryst size, mm	0.24 × 0.19 × 0.05	0.24 × 0.09 × 0.09
T, K	193(2)	173(2)
wavelength,^{b} Å	0.71073	0.71073
μ, mm^{-1}	14.11	16.02
R1(wR2)^{c,d}	0.0485 (0.1366)^e	0.0451 (0.0972)^f
R1(wR2)^g	0.0650 (0.1492)	0.0985 (0.1091)

^{a} Including solvate molecules. ^{b} Mo Kα, graphite monochromator. ^{c} R1 = $\sum(||F_o| - |F_c||)/\sum|F_o|$. ^{d} wR2 = $[\sum[w(F_o^2 - F_c^2)^2]/\sum[w(F_o^2)^2]]^{1/2}$, $w = 1/[\sigma^2(F_o^2) + [(ap)^2 + bp]$, where $p = [\max (F_o^2, 0) + 2F_c^2]/3$. ^{e} 10 510 reflections with $I > 2\sigma(I)$. ^{f} 11 961 reflections with $I > 2\sigma(I)$. ^{g} All data.

eicosane to prevent torquing. Magnetization versus field and temperature data were fit using the program MAGNET.[12] For single-crystal micro-SQUID studies, crystals maintained in mother liquor to avoid degradation were covered in grease for protection during the transfer to the micro-SQUID and subsequent cooling.

Results and Discussion

Syntheses. Our strategy for investigating the reactions of phenylphosphinic acid (PhHPO$_2$H) with Mn sources was the same as that employed previously for diphenylphosphinic acid (Ph$_2$PO$_2$H), namely, reaction with preformed [Mn$_{12}$O$_{12}$(O$_2$-CR)$_{16}$(H$_2$O)$_4$] complexes in MeCN.[4d,7] Thus, [Mn$_{12}$O$_{12}$(O$_2$-CEt)$_{16}$(H$_2$O)$_3$] (**1**), freshly recrystallized from CH$_2$Cl$_2$/hexanes, was dissolved in MeCN and treated with 8 equiv of PhHPO$_2$H. After 12 h, the resulting brown slurry was filtered to separate a deep-brown solution from a light brown powder; we have been unable to crystallize and characterize the latter. However, slow concentration of the filtrate and refiltering when more light brown powder was observed after a few days, eventually led to growth of dark brown/black, well-formed crystals of **2·6MeCN·2CH$_2$Cl$_2$** after several weeks, contaminated with some brown powder. The yield was low (typically <5%), but the synthesis is reproducible. The product was subsequently identified by X-ray crystallography as [Mn$_{22}$O$_{12}$(O$_2$CEt)$_{22}$(O$_3$PPh)$_8$(H$_2$O)$_8$], and it became apparent that the product contained phenylphosphonate (PhPO$_3^{2-}$) groups, oxidized forms of the added PhHPO$_2$H, which rationalizes the slow formation of **2** and its low yield; it is clearly a minor product forming during the long crystallization period.

Once the unusual structure of **2** had been established (vide infra), we explored a number of reactions modified in the reagent ratio, solvent, or both in an attempt to improve the yield. When the reaction was carried out in a 1:1 MeCN/CH$_2$Cl$_2$ mixture, the reaction proceeded analogously and,

(12) Davidson, E. R., Indiana University, Bloomington, 1999.

after similar workup to **2**, gave dark brown/black crystals in a higher yield and in a shorter crystallization time than the MeCN reaction system. We initially thought this product was also **2**, but it turned out, upon crystallographic identification, to instead be a slightly modified form of formula $[Mn_{22}O_{12}(O_2CEt)_{20}(O_3PPh)_8(O_2PPhH)_2(H_2O)_8]_n$ (**3**). Complex **3** is overall similar to **2** in that both contain structurally similar Mn_{22} units (vide infra), with the two main differences being that (i) **3** still contains some unoxidized $PhHPO_2^-$ groups and (ii) **3** is a one-dimensional polymer of Mn_{22} units bridged by carboxylate groups.

The formation of the Mn_{22} complexes **2** and **3** was obviously unexpected because we had been anticipating only a ligand substitution reaction on the Mn_{12} complex **1** to give a mixed a carboxylate/phenylphosphinate product, similar perhaps to $[Mn_{12}O_{12}(O_2CMe)_8(O_2PPh_2)_8(H_2O)_4]$ and related derivatives obtained with diphenylphosphinic acid.[4d,7] Clearly the enhanced vulnerability to oxidation of the P–H bond versus the P–Ph bond is an important factor in the formation of **2** and **3**, albeit in low to average yields. Indeed, the plentiful light brown powder, the main product of these reactions, is perhaps the expected carboxylate/phenylphosphinate product, but we have no further information on its exact formulation except that IR spectra confirm that it does contain both types of organic groups.

Note that the in situ oxidative conversion of added $PhHPO_2H$ into a $PhPO_3^{2-}$ ligand is with precedent, having been seen in reactions somewhat similar to those that yield **2** and **3**. For example, the reaction of $[Mn_3O(O_2CPh)_6(py)_2(H_2O)]$ with $PhHPO_2H$ leads to the complex $[Mn_6O_2(O_3PPh)_2(O_2PHPh)_2(O_2CPh)_8(py)_2]$ in low yield.[13] The oxidation of $PhHPO_2^-$ to $PhPO_3^{2-}$ likely involves atmospheric O_2 and perhaps water molecules, but the low yields make it difficult to analyze further. In any case, the reaction mixtures are clearly very complicated and almost certainly contain a number of species in equilibrium, which would also rationalize the formation of **3** not **2** when the reaction between **1** and $PhHPO_2H$ was carried out in $MeCN/CH_2Cl_2$ instead of just MeCN; factors such as relative solubility, lattice energies, crystallization kinetics, and others will determine the exact equilibrium species to crystallize. Note also that there are already in the literature compounds containing RPO_3^{2-} groups bridging Mn ions into one-dimensional polymer chains, but molecular Mn complexes containing such groups are rare.[13,15b,d,g] In general, phosphinate and phosphonate ligands are well explored for many metals,[13–16] and some have turned out to be SMMs.[15b,e,g] Finally, we also explored

the use of $[Mn_{12}O_{12}(O_2CR)_{16}(H_2O)_4]$ (R = Me, Ph) complexes in reactions with $PhHPO_2H$ but, in these cases, were unable to isolate any crystalline products for characterization.

The analytical data for complex **2**, obtained on samples dried overnight under vacuum, agreed perfectly with a formula containing only two water molecules, that is, $[Mn_{22}O_{12}(O_2CEt)_{22}(O_3PPh)_8(H_2O)_2]$, indicating bound water molecules to have been removed by the vacuum. Since six of the eight water molecules in **2** are attached to Mn^{II} ions, it is reasonable to conclude that these were the ones lost, with those on Mn^{III} ions being more firmly held. For complex **3**, vacuum-dried materials were very hygroscopic, as established for example by monitoring the progressive gain in weight with time, and we were unable to obtain an acceptable elemental analysis, even after multiple attempts. This hygroscopicity is consistent with the extensive channels in the crystal (Figure S1), which are full of solvent molecules until dried. Therefore, for the magnetic studies of **3** to be described below, we placed freshly vacuum-dried solid into a protective eicosane matrix, and we assumed that the solid was solvent-free for the purposes of calculating molecular weights.

Description of Structures. ORTEP representations of complex **2** and its labeled asymmetric unit are shown in Figures 1 and 2, respectively. Selected interatomic distances are listed in Table 2. $[Mn_{22}O_{12}(O_2CEt)_{22}(O_3PPh)_8(H_2O)_8]\cdot$ $6MeCN\cdot2CH_2Cl_2$ crystallizes in the triclinic space group $P\bar{1}$ with the mixed-valence (Mn^{III}_{18}, Mn^{II}_4) molecule lying on an inversion center. The structure consists of two Mn^{III}_9 units linked through four additional Mn^{II} atoms. Each $[Mn_9(\mu_3\text{-}O^{2-})_6]^{15+}$ core can be described as "a basket with a handle": the $[Mn_7(\mu_3\text{-}O^{2-})_4]$ basketlike subunit consists of two $[Mn_4(\mu_3\text{-}O^{2-})_2]$ butterfly units (atoms Mn1, 2, 4, 7 and Mn1, 3, 5, 8) fused at Mn1. The resultant $[Mn_3O_4]$ base is almost linear with a Mn2–Mn1–Mn3 angle of 175°. The $[Mn_4(\mu_3\text{-}O^{2-})_2]$ units are structurally similar to those in discrete tetranuclear butterfly complexes containing the same $[Mn_4(\mu_3\text{-}O^{2-})_2]^{8+}$ core.[17] The "handle" consists of atoms Mn6 and Mn9, which are connected to the basket by two additional $\mu_3\text{-}O^{2-}$ ions, O17 and O30. The two $[Mn_9(\mu_3\text{-}O^{2-})_6]^{15+}$ units are then linked by four Mn atoms, Mn10 and Mn11 (and their symmetry partners), via bridging through carboxylate and phosphonate groups, giving the complete Mn_{22} unit.

(13) Brechin, E. K.; Coxall, R. A.; Parkin, A.; Parsons, S.; Tasker, P. A.; Winpenny, R. E. P. *Angew. Chem., Int. Ed.* **2001**, *40*, 2700 and references therein.

(14) (a) Yucesan, G.; Yu, M. H.; Ouellette, W.; O'Connor, C. J.; Zubieta, J. *Cryst. Eng. Commun.* **2005**, *7*, 480. (b) Yucesan, G.; Golub, V.; O'Connor, C. J.; Zubieta, J. *Dalton Trans.* **2005**, 2241. (c) Finn, R. C.; Burkholder, E.; Zubieta, J. *Perspect Supramol. Chem.* **2003**, *7*, 241. (d) Finn, R. C.; Zubieta, J.; Haushalter, R. C. *Prog. Inorg. Chem.* **2003**, *51*, 421. (e) Finn, R. C.; Zubieta, J. *Inorg. Chem.* **2001**, *40*, 2466. (f) Salta, J.; Zubieta, J. *J. Cluster Sc.* **1996**, *7*, 531. (g) Salta, J.; Chen, Q.; Zubieta, J. *Angew. Chem., Int. Ed. Engl.* **1994**, *33*, 757. (h) Soghomonian, V.; Haushalter, R. C.; Zubieta, J. *Chem. Mater.* **1995**, *7*, 1648. (i) Soghomonian, V.; Chen, Q.; Haushalter, R. C.; Zubieta, J. *Angew. Chem., Int. Ed. Engl.* **1993**, *32*, 610.

(15) (a) Khanra, S.; Kloth, M.; Mansaray, H.; Muryn, C. A.; Tuna, F.; Sanudo, E. C.; Helliwell, M.; McInnes, E. J. L.; Winpenny, R. E. P. *Angew. Chem., Int. Ed.* **2007**, *46*, 5568. (b) Maheswaran, S.; Chastanet, G.; Teat, S. J.; Mallah, T.; Sessoli, R.; Wernsdorfer, W.; Winpenny, R. E. P. *Angew. Chem., Int. Ed.* **2005**, *44*, 5044. (c) Tolis, E. I.; Helliwell, M.; Langley, S.; Raftery, J.; Winpenny, R. E. P. *Angew. Chem., Int. Ed.* **2003**, *42*, 3804. (d) Shanmugam, M.; Shanmugam, M.; Chastanet, G.; Sessoli, R.; Mallah, T.; Wernsdorfer, W.; Winpenny, R. E. P. *J. Mater. Chem.* **2006**, *16*, 2576. (e) Langley, S. J.; Helliwell, M.; Sessoli, R.; Rosa, P.; Wernsdorfer, W.; Winpenny, R. E. P. *Chem. Commun.* **2005**, 5029. (f) Langley, S.; Helliwell, M.; Raftery, J.; Tolis, E. I.; Winpenny, R. E. P. *Chem. Commun.* **2004**, 142. (g) Shanmugam, M.; Chastanet, G.; Mallah, T.; Sessoli, R.; Teat, S. J.; Timco, G. A.; Winpenny, R. E. P. *Chem.—Eur. J.* **2006**, *12*, 8777.

(16) (a) Konar, S.; Bhuvanesh, N.; Clearfield, A. *J. Am. Chem. Soc.* **2006**, *128*, 9604. (b) Bakhmutova, E. K.; Ouyang, X.; Medvedev, D. G.; Clearfield, A. *Inorg. Chem.* **2003**, *42*, 7046. (c) Clearfield, A. *J. Alloys Compds.* **2006**, *418*, 128. (d) Cabeza, A.; Aranda, M. A. G.; Bruque, S.; Poojary, D. M.; Clearfield, A. *Mater. Res. Bull.* **1998**, *33*, 1265.
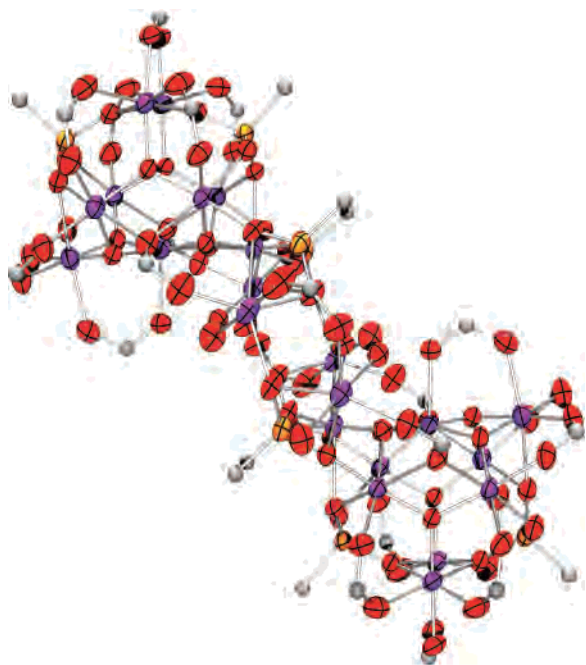
Figure 1. ORTEP representation of centrosymmetric complex **2** at the 50% probability level. For clarity, the Et groups of the $EtCO_2^-$ ligands have been removed, and only the *ipso* carbon atom of each Ph ring is shown. Color code: Mn violet; O red; P orange; C gray.
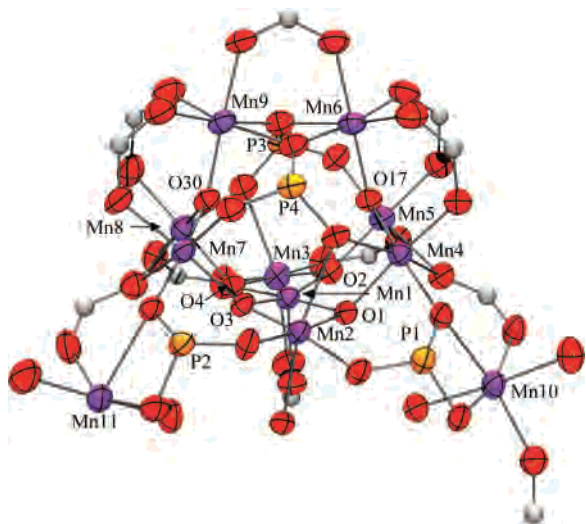

Figure 2. Labeled ORTEP representation at the 50% probability level of the asymmetric unit of complex **2**. For clarity, all Ph rings and the Et groups of the $EtCO_2^-$ ligands have been removed. Color code: Mn violet; O red; P orange; C gray.

Peripheral ligation around each $[Mn_9(\mu_3\text{-}O^{2-})_6]^{15+}$ unit and between them and the central Mn10 and Mn11 atoms is provided by a total of twenty-two $EtCO_2^-$ and eight $PhPO_3^{2-}$ bridging groups and eight terminal H_2O molecules, the latter on Mn2, Mn10, and Mn11. The $EtCO_2^-$ and $PhPO_3^{2-}$ groups

(17) (a) Vincent, J. B.; Christmas, C.; Chang, H.-R.; Li, Q.; Boyd, P. D. W.; Huffman, J. C.; Hendrickson, D. N.; Christou, G. *J. Am. Chem. Soc.* **1989**, *111*, 2086. (b) Vincent, J. B.; Christmas, C.; Huffman, J. C.; Christou, G.; Chang, H.-R.; Hendrickson, D. N. *J. Chem. Soc., Chem. Commun.* **1987**, 236. (c) Libby, E.; McCusker, J. K.; Schmitt, E. A.; Folting, K.; Hendrickson, D. N.; Christou, G. *Inorg. Chem.* **1991**, *30*, 3486. (d) Wemple, M. W.; Tsai, H.-L.; Wang, S.; Claude, J.-P.; Streib, W. E.; Huffman, J. C.; Hendrickson, D. N.; Christou, G. *Inorg. Chem.* **1996**, *35*, 6450.

Table 2. Selected Interatomic Distances (Å) for Complex **2**·6MeCN·2CH₂Cl₂

Mn1−O4	1.888(4)	Mn5−O2	1.857(4)
Mn1−O2	1.895(3)	Mn5−O17	1.937(3)
Mn1−O3	1.898(3)	Mn5−O18	1.948(4)
Mn1−O1	1.904(3)	Mn5−O20	1.977(4)
Mn1−O5	2.132(4)	Mn5−O19	2.115(4)
Mn2−O3	1.889(3)	Mn5−O16	2.292(4)
Mn2−O9	1.906(3)	Mn6−O17	1.862(3)
Mn2−O7	1.926(3)	Mn6−O23	1.944(4)
Mn2−O1	1.933(3)	Mn6−O25	1.948(4)
Mn2−O8	2.275(4)	Mn6−O22	1.961(4)
Mn2−O6	2.340(4)	Mn6−O21	2.123(5)
Mn3−O2	1.878(4)	Mn6−O24	2.248(4)
Mn3−O4	1.899(3)	Mn7−O3	1.915(3)
Mn3−O11	1.932(4)	Mn7−O30	1.924(3)
Mn3−O12	1.950(4)	Mn7−O26	1.930(3)
Mn3−O10	2.181(4)	Mn7−O29	1.952(4)
Mn3−O13	2.388(4)	Mn7−O28	2.104(4)
Mn4−O1	1.913(3)	Mn7−O27	2.288(4)
Mn4−O17	1.913(3)	Mn8−O4	1.887(4)
Mn4−O15	1.924(4)	Mn8−O30	1.919(4)
Mn4−O14	1.961(3)	Mn8−O32	1.930(4)
Mn4−O6	2.242(4)	Mn8−O31	1.965(4)
Mn4−O16	2.340(4)	Mn8−O13	2.177(4)
Mn9−O30	1.862(4)	Mn8−O27	2.266(4)
Mn9−O33	1.960(4)	Mn10−O37	2.201(4)
Mn9−O24	1.962(4)	Mn10−O36	2.282(3)
Mn9−O34	1.965(4)	Mn10−O14	2.291(4)[a]
Mn9−O35	2.131(5)	Mn11−O42	2.107(5)[a]
Mn9−O22	2.214(4)	Mn11−O41	2.116(4)[a]
Mn10−O39	2.100(4)	Mn11−O36¢	2.158(4)[a]
Mn10−O40	2.117(4)	Mn11−O43	2.192(4)[a]
Mn10−O38	2.182(4)	Mn11−O44	2.241(4)[a]
Mn4···Mn5	3.2319(12)	Mn11−O26	2.434(4)[a]
Mn2···Mn4	3.1714(12)	Mn1···Mn2	2.8305(11)
Mn2···Mn4	3.1714(12)	Mn6···Mn9	3.1998(14)
Mn3···Mn8	3.1142(13)	Mn6···Mn9	3.1998(14)
Mn1···Mn3	2.7801(11)	Mn7···Mn8	3.1667(12)

[a] Mn10 and Mn11 are Mn^{II} atoms; all others are Mn^{III}.

adopt a variety of bridging modes, and these are shown in Figure 3. Eighteen $EtCO_2^-$ groups bridge two Mn atoms in the common $\eta^1{:}\eta^1{:}\mu$ mode (**I**), while the remaining four bridge three Mn atoms in the rarer $\eta^1{:}\eta^2{:}\mu_3$ mode (**II**). The $PhPO_3^{2-}$ groups adopt three different bridging modes: four (P3 and P4) bridge five Mn atoms in a $\eta^1{:}\eta^2{:}\eta^2{:}\mu_5$ mode (**III**), two (P1) bridge four Mn atoms in a $\eta^1{:}\eta^2{:}\eta^2{:}\mu_4$ mode (**IV**), and the remaining two (P2) bridge three Mn atoms in a $\eta^1{:}\eta^1{:}\eta^2{:}\mu_3$ mode (**V**).

The Mn oxidation states were established qualitatively by inspection of the metric parameters and were confirmed quantitatively by bond valence sum (BVS) calculations shown in Table 3.[18] These confirmed the trapped-valence Mn^{III}_{18}, Mn^{II}_4 oxidation state description with Mn10 and Mn11 being Mn^{II}. The other Mn atoms are Mn^{III}, which is consistent with the Jahn−Teller (JT) axial elongations that they all display (except Mn1), as expected for high-spin d^4 ions in near-octahedral geometry. Atom Mn1 is five-coordinate with square pyramidal geometry ($\tau = 0.02$, where τ is 0 and 1 for ideal square pyramidal and trigonal bipyramidal geometries, respectively).[19] The protonation level of O^{2-} groups were determined by charge balance considerations and BVS calculations,[18] as shown in Table 3. The

(18) Liu, W.; Thorp, H. H. *Inorg. Chem.* **1993**, *32*, 4102.
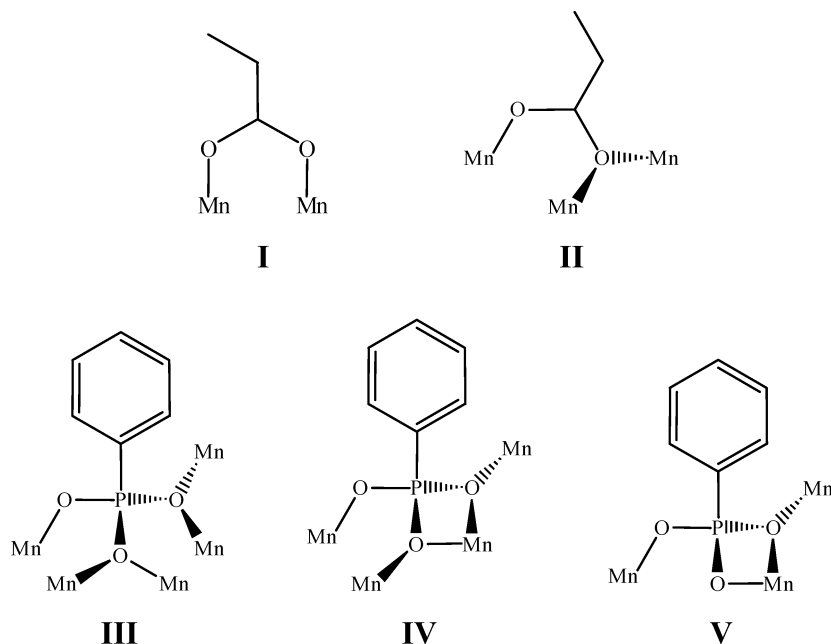(19) Addison, A. W.; Rao, T. N.; Reedijk, J.; Rijn J.; Verschoor, G. C. *J. Chem. Soc., Dalton Trans.* **1984**, 1349.

Figure 3. Bridging modes displayed by the $EtCO_2^-$ and $PhPO_3^{2-}$ groups in complexes **2** and **3**.

Table 3. Bond Valence Sums for Mn[a] and Selected Oxygen[b] Atoms in Complex **2**

atom	Mn²⁺	Mn³⁺	Mn⁴⁺
Mn1	3.18	2.90	3.05
Mn2	3.14	2.88	3.02
Mn3	3.19	2.91	3.06
Mn4	3.07	2.80	2.94
Mn5	3.21	2.94	3.08
Mn6	3.24	2.97	3.11
Mn7	3.20	2.93	3.08
Mn8	3.18	2.91	3.06
Mn9	3.20	2.93	3.08
Mn10	1.91	1.75	1.83
Mn11	1.91	1.74	1.83

atom	BVS	assignment
O1	1.72	O²⁻
O2	1.93	O²⁻
O3	1.80	O²⁻
O4	1.85	O²⁻
O17	1.79	O²⁻
O19	1.80	O²⁻

[a] The underlined value is the one closest to the charge for which it was calculated. The oxidation state of a particular atom can be taken as the nearest whole number to the underlined value. [b] BVS values for O atoms of O²⁻, OH⁻, and H₂O groups are typically 1.8−2.0, 1.0−1.2, and 0.2−0.4, respectively, but can be altered somewhat by hydrogen bonding.

slightly low BVS value of O1 (1.72) is caused by an O···H−O hydrogen bond with terminal water O37 on Mn10 (O1··O37 = 2.874 Å).

The Mn₉ subunits of **2** are similar to those found in two discrete enneanuclear Mn₉ complexes already in the literature. These are $[Mn_9O_7(O_2CPh)_{13}(py)_2]$, which was obtained from the reaction of $[Mn_3O(O_2CPh)_6(py)_2(H_2O)]$ with the oxygen transfer reagent iodosobenzene (PhIO),[20] and $[Na_2-Mn_9O_7(OCPh)_{15}(MeCN)_2]$, which was obtained from the reaction of $(NBu^n_4)[Mn_4O_2(O_2CPh)_9(H_2O)]$ with dibenzoylperoxide $[(PhCO)_2O_2]$.[21,22] The Mn₁₈ complex $[Mn_{18}O_{14}(O_2-$

$CPh-p-OMe)_{26}(bpy)_2]$ was obtained from the reaction of $(NBu^n_4)[Mn_4O_2(O_2Ph-p-OMe)_9(H_2O)]$ with 4,4′-bipyridine (bpy) and is even more structurally related to **2** in that it contains two Mn₉ units joined together by bridging bpy ligands.[23] In all these complexes, the Mn₉ topology is very similar to that in **2**, particularly, with respect to the basket-with-handle appearance and the central $[Mn_3O_4]$ base with the central Mn being 5-coordinate. However, in the previous compounds, there is seventh μ_3-O²⁻ ion in the center of the core bridging the central Mn with the two handle Mn atoms. This causes the $[Mn_3O_4]$ base to be bent (~145°) rather than near-linear as in **2**. The absence of a seventh μ_3-O²⁻ ion in the center of the core means the apex of the square pyramid of the central Mn1 is on the outside, a situation more analogous to the corresponding Mn atom in the somewhat related Mn₈ core of $(^nBu_4N)[Mn_8O_6Cl_6(O_2CPh)_7(H_2O)_2]$, which has the same basket of two fused $[Mn_4O_2]$ butterfly units (but only one additional Mn atom) and contains a near-linear $[Mn_3O_4]$ base with a Mn−Mn−Mn angle of 172.5°.[22]

$[Mn_{22}O_{12}(O_2CEt)_{20}(O_3PPh)_8(O_2PPhH)_2(H_2O)_8]_n$·$7n$MeCN (**3**) crystallizes in the monoclinic space group $P2_1/n$ as one-dimensional chains of Mn₂₂ units. A section of the chain containing two Mn₂₂ units is shown in Figure 4, and the labeled asymmetric unit is shown in Figure 5. Selected interatomic distances are listed in Table 4. The structure of **3** is very similar to that of **2**, with the major difference being that **3** is a one-dimensional polymer of Mn₂₂ units linked by two carboxylate groups. BVS calculations again indicate a trapped-valence Mn$^{III}_{18}$, Mn$^{II}_4$ oxidation state situation. The Mn₉ core has the same structure as that in **2** (Figure 2), with

(20) Low, D. W.; Eichhorn, D. M.; Draganescu, A.; Armstrong, W. H. *Inorg. Chem.* **1991**, *30*, 878.

(21) Wang, S.; Huffman, J. C.; Folting, K.; Streib, W. E.; Lobkovsky, E. B.; Christou, G. *Angew. Chem., Int. Ed. Engl.* **1991**, *30*, 1672.

(22) Tsai, H.-L.; Wang, S.; Folting, K.; Streib, W. E.; Hendrickson, D. N.; Christou, G. *J. Am. Chem. Soc.* **1995**, *117*, 2503.

(23) Eppley, H. J.; deVries, N.; Wang, S.; Aubin, S. M.; Tsai, H.-L.; Folting, K.; Hendrickson, D. N.; Christou, G. *Inorg. Chim. Acta* **1997**, *263*, 323.
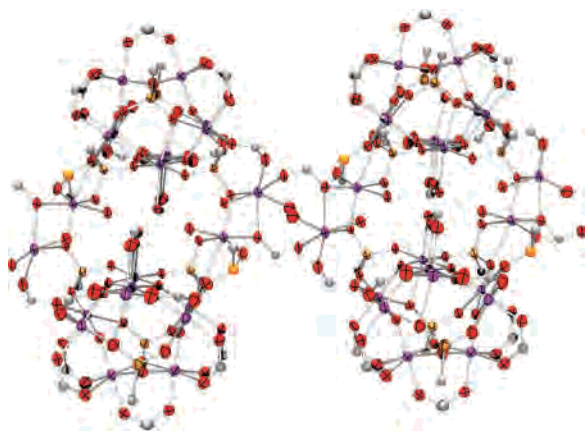
Figure 4. ORTEP representation at the 50% probability level of two [Mn$_{22}$] repeating units of complex **3**. For clarity, the Et groups of the EtCO$_2^-$ ligands have been removed, and only the *ipso* carbon atom of each Ph ring is shown. Color code: Mn violet; O red; P orange; C gray.
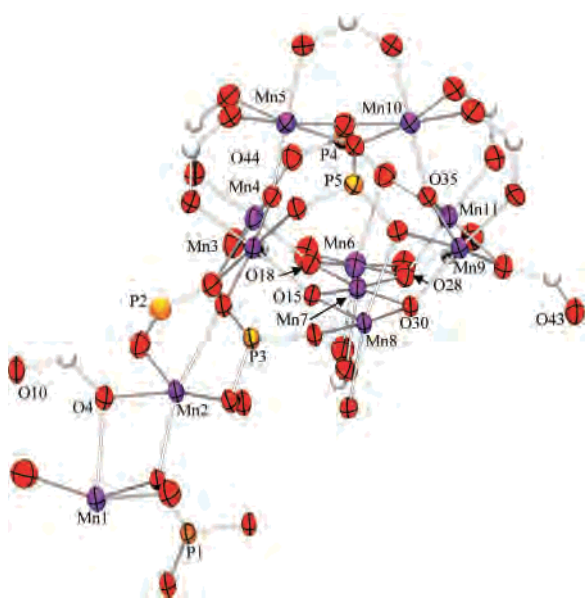

Figure 5. Labeled ORTEP representation at the 50% probability level of the asymmetric unit of complex **3**. For clarity, all Ph rings and the Et groups of the EtCO$_2^-$ ligands have been removed. Color code: Mn violet; O red; P orange; C gray.

Table 4. Selected Interatomic Distances (Å) for Complex **3**·7MeCN

Mn1−O43′	2.141(3)^a	Mn5−O44	1.838(2)
Mn1−O10′	2.144(3)^a	Mn5−O24	1.935(3)
Mn1−O2	2.202(3)^a	Mn5−O22	1.980(3)
Mn1−O1	2.226(3)^a	Mn5−O20	2.002(3)
Mn1−O3	2.262(3)^a	Mn5−O23	2.132(3)
Mn1−O4	2.327(3)^a	Mn5−O21	2.200(3)
Mn2−O7	2.085(3)^a	Mn6−O18	1.869(3)
Mn2−O3	2.122(2)^a	Mn6−O28	1.885(3)
Mn2−O4	2.170(3)^a	Mn6−O25	1.925(3)
Mn2−O6	2.198(3)^a	Mn6−O27	1.954(3)
Mn2−O5	2.206(3)^a	Mn6−O26	2.181(3)
Mn2−O12	2.441(2)^a	Mn6−O40	2.436(3)
Mn3−O44	1.891(3)	Mn7−O18	1.887(3)
Mn3−O15	1.919(2)	Mn7−O30	1.897(3)
Mn3−O12	1.942(3)	Mn7−O15	1.902(3)
Mn3−O11	1.945(3)	Mn7−O28	1.908(3)
Mn3−O14	2.130(2)	Mn7−O29	2.150(3)
Mn3−O13	2.299(3)	Mn8−O15	1.908(3)
Mn4−O18	1.870(3)	Mn8−O32	1.909(2)
Mn4−O44	1.916(3)	Mn8−O30	1.916(3)
Mn4−O16	1.923(3)	Mn8−O8′	1.925(3)
Mn4−O19	1.963(3)	Mn8−O31	2.263(2)
Mn4−O17	2.142(3)	Mn8−O33	2.347(2)
Mn4−O13	2.371(3)	Mn10−O35	1.877(2)
Mn9−O9′	1.911(3)	Mn10−O36	1.954(3)
Mn9−O30	1.916(2)	Mn10−O21	1.981(3)
Mn9−O34	1.931(2)	Mn10−O37	2.004(3)
Mn9−O35	1.940(3)	Mn10−O38	2.086(3)
Mn9−O33	2.234(2)	Mn10−O20	2.125(3)
Mn9−O39	2.252(3)	Mn11−O42	1.964(3)
Mn11−O28	1.866(3)	Mn11−O40	2.209(3)
Mn11−O41	1.926(3)	Mn11−O39	2.224(3)
Mn11−O35	1.928(3)		
Mn3···Mn4	3.2254(9)	Mn7···Mn8	2.8492(9)
Mn4···Mn5	3.2398(8)	Mn8···Mn9	3.1483(8)
Mn5···Mn10	3.1700(8)	Mn9···Mn11	3.1603(9)
Mn6···Mn7	2.8026(10)	Mn6···Mn11	3.0808(8)

^{a} Mn1 and Mn2 are Mn^{II} atoms; all others are Mn^{III}.

to molecular and chain structures for **2** and **3**, respectively. Examination of the packing of **3** revealed extensive channels between chains containing MeCN molecules (Figure S1), consistent with the hygroscopic nature of complex **3**.

Complexes **2** and **3** represent only the second and third examples of a Mn$_{22}$ cluster. The first was [Mn$_{22}$O$_6$(OMe)$_{14}$(O$_2$-CMe)$_{16}$(thp)$_8$(HIm)$_2$], where thp^{3-} is the triply deprotonated anion of 1,1,1-tris(hydroxymethyl)propane, and HIm is imidazole.[24] Only a very few larger Mn clusters have been reported to date, Mn$_{84}$,[6f] Mn$_{70}$,[25] Mn$_{40}$,[26] Mn$_{32}$,[27] Mn$_{30}$,[6a,e] two Mn$_{26}$,[28] and two Mn$_{25}$.[29]

the central five-coordinate Mn (Mn7) again being square pyramidal ($\tau = 0.02$). One slight difference between **2** and **3** is found in the $\eta^1:\eta^2:\eta^2:\mu_5$-bridging PhPO$_3^{2-}$ groups in mode **III** (P3/P4 for **2**, P4/P5 for **3**), which are disposed differently relative to each other; the pair is related by a virtual C_2 axis in **2** and a virtual mirror plane in **3**. Complex **2** possesses a μ_3-EtCO$_2^-$ group bridging the Mn$_9$ core to Mn11 (Figure 2), but in **3**, there is a μ_3-PhHPO$_2^-$ group. This PhHPO$_2^-$ group increases the Mn2···Mn3 distance to 3.920 Å versus the Mn7···Mn11 distance of 3.876 Å in **2**. In addition, the Mn^{II}−Mn^{II} distance of **3** is 3.486 Å, much shorter than the distance of 3.725 Å in **2**, which allows the bridging EtCO$_2^-$ group to become triply bridging, with O4 bridging Mn1 and Mn2, and freeing O10 to link to the symmetry-related Mn1 of a second Mn$_{22}$ unit giving the one-dimensional chain. The structural differences between **2** and **3** are consequently minor, differing in the bridging ligands involving primarily the Mn^{II} atoms. Nevertheless they lead

(24) Murugesu, M.; Raftery, J.; Wernsdorfer, W.; Christou, G.; Brechin, E. K. *Inorg. Chem.* **2004**, *43*, 4203.
(25) Vinslava, A.; Tasiopoulos, A. J.; Wernsdorfer, W.; Abboud, K. A.; Christou, G. Unpublished work.
(26) Moushi, E.; Lampropoulos, C.; Wernsdorfer, W.; Nastopoulos, V.; Christou, G.; Tasiopoulos, A. J. *Inorg. Chem.* **2007**, *46*, 3795.
(27) (a) Scott, R. T. W.; Milios, C. J.; Vinslava, A.; Lifford, D.; Parsons, S.; Wernsdorfer, W.; Christou, G.; Brechin, E. K. *Dalton Trans.* **2006**, 3161. (b) Scott, R. T. W.; Parsons, S.; Murugesu, M.; Wernsdorfer, W.; Christou, G.; Brechin, E. K. *Angew. Chem., Int. Ed.* **2005**, 6540.
(28) (a) Jones, L. F.; Brechin, E. K.; Collison, D.; Harrison, A.; Teat, S. J.; Wernsdorfer, W. *Chem. Commun.* **2002**, 2974. (b) Dendrinou-Samara, C.; Alexiou, M.; Zaleski, C. M.; Kampf, J. W.; Kirk, M. L.; Kessissoglou, D. P.; Pecoraro, V. L. *Angew. Chem., Int. Ed.* **2003**, *42*, 3763.
(29) (a) Murugesu, M.; Habrych, M.; Wernsdorfer, W.; Abboud, K. A.; Christou, G. *J. Am. Chem. Soc.* **2004**, *126*, 4766. (b) Stamatatos, T. C.; Abboud, K. A.; Wernsdorfer, W.; Christou, G. *Angew. Chem. Int. Ed.* **2007**, *46*, 884. (c) Stamatatos, T. C.; Abboud, K. A.; Wernsdorfer, W.; Christou, G. *Polyhedron* **2007**, *26*, 2095.
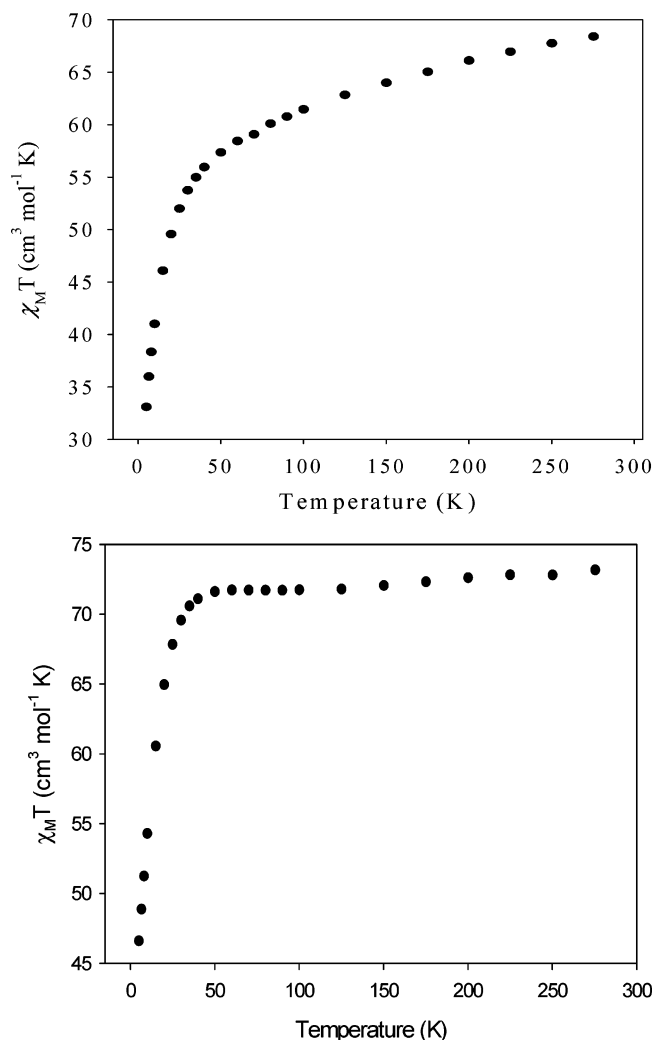
Figure 6. Plots of dc $\chi_M T$ vs T for complexes **2** (top) and **3** (bottom).

Magnetochemistry. DC Magnetic Susceptibility Studies. Solid-state, variable-temperature dc magnetic susceptibility measurements were performed on vacuum-dried samples of **2** and **3**, suspended in eicosane to prevent torquing. The DC magnetic susceptibility (χ_M) data for **2** and **3** were collected in the 5.0−275 K range in a 0.10 T magnetic field and are plotted as $\chi_M T$ versus T in Figure 6. The $\chi_M T$ for **2** decreases with decreasing temperature from 68.0 cm³ K mol⁻¹ at 275 K to 55.0 cm³ K mol⁻¹ at 35 K before rapidly decreasing to 33.1 cm³ K mol⁻¹ at 5.0 K. The spin-only ($g = 2$) value for a cluster containing 18 Mn^III and 4 Mn^II non-interacting ions is 71.5 cm³ K mol⁻¹, so the observed value at 275 K suggests the presence of dominant antiferromagnetic interactions within the molecule. However, the $\chi_M T$ does not drop to near zero at the lowest temperatures suggesting that **2** may possess a relatively high-spin ground state. The $\chi_M T$ for **3** is 73.2 cm³ K mol⁻¹, and it decreases slowly to 71.6 cm³ K mol⁻¹ at 50 K before rapidly decreasing to 46.6 cm³ K mol⁻¹ at 5.0 K. Again, $\chi_M T$ decreases rapidly at the lowest temperatures but does not drop to near zero at 5.0 K.

To probe the ground state of complex **2**, DC magnetization (M) data were collected in the 0.1−7 T (1−70 kG) field range and the 1.80−10.00 K temperature range. Attempts were made to fit the data using the program MAGNET,[12]

which assumes that only the ground state is populated at these temperatures, includes axial ZFS ($D\hat{S}_z^2$) and the Zeeman interaction with the applied field, and carries out a full powder average. The corresponding spin Hamiltonian is given in eq 1. However, it was not possible to obtain a good

$$\mathscr{H} = D\hat{S}_z^2 + g\mu_B\mu_0\hat{S}H \tag{1}$$

fit when all the data collected at all fields were used. In our experience, the usual reason for this is the presence of low-lying excited states because (i) the excited states are close enough to the ground state that they have a nonzero Boltzmann population even at the low temperatures used in the magnetization data collection and (ii) even excited states that are more separated from the ground state but have an S value greater than that of the ground-state become populated as their larger M_S levels rapidly decrease in energy in the applied magnetic field and approach (or even cross) those of the ground state. Either (or both) of these two effects will lead to poor fits because the fitting program assumes population of only the ground state. A large density of low-lying excited states is expected for such a large nuclearity cluster as **2**, especially given that it has a significant content of Mn^II ions, which give weak exchange couplings. As we have described elsewhere,[6e,6g,30] one way around effect ii is to use only data collected at low fields. Indeed, two reasonable fits of the magnetization data could be achieved using only data collected in fields up to 0.5 T, suggesting that effect ii is indeed the main cause of the fitting problems. The two fits were of comparable quality, with fit parameters $S = 7$, $D = -0.16$ cm⁻¹, $g = 2.1$ and $S = 8$, $D = -0.13$ cm⁻¹, and $g = 1.83$. The data and former fit are shown as a reduced magnetization ($M/N\mu_B$) versus H/T plot in the Supporting Information (Figure S2), where N is Avogadro's number and μ_B is the Bohr magneton. The reduced magnetization fits thus indicate that the ground state of **2** is $S = 7$ or 8, but the quoted D and g values must not be taken as accurate. A better determination of the true ground state of **2** can be obtained using AC susceptibility measurements because, as we have stated elsewhere on multiple occasions,[6e,g,29,30] this removes the complications from the applied DC field. Such AC experiments also allow assessment of whether a compound might exhibit the slow magnetization of a single-molecule magnet (SMM). A more reliable value for D will also be provided below (vide infra).

AC Magnetic Susceptibility Studies. In an AC susceptibility experiment, a weak field (typically 1−5 G) oscillating a particular frequency (ν) is applied to a sample to probe the dynamics of the magnetization (magnetic moment) relaxation. The AC susceptibility studies were performed on vacuum-dried polycrystalline samples of **2** and **3** in the temperature range 1.8−10 K in a zero DC field and in a 3.5 G AC field oscillating at frequencies in the 5−1500 Hz range.

(30) (a) Sanudo, E. C.; Wernsdorfer, W.; Abboud, K. A.; Christou, G. *Inorg. Chem.* **2004**, *43*, 4137. (b) King, P.; Wernsdorfer, W.; Abboud, K. A.; Christou, G. *Inorg. Chem.* **2005**, *44*, 8659. (c) Tasiopoulos, A. J.; Wernsdorfer, W.; Abboud, K. A.; Christou, G. *Inorg. Chem.* **2005**, *44*, 6324. (d) Boskovic, C.; Wernsdorfer, W.; Folting, K.; Huffman, J. C.; Hendrickson, D. N.; Christou, G. *Inorg. Chem.* **2002**, *41*, 5107.
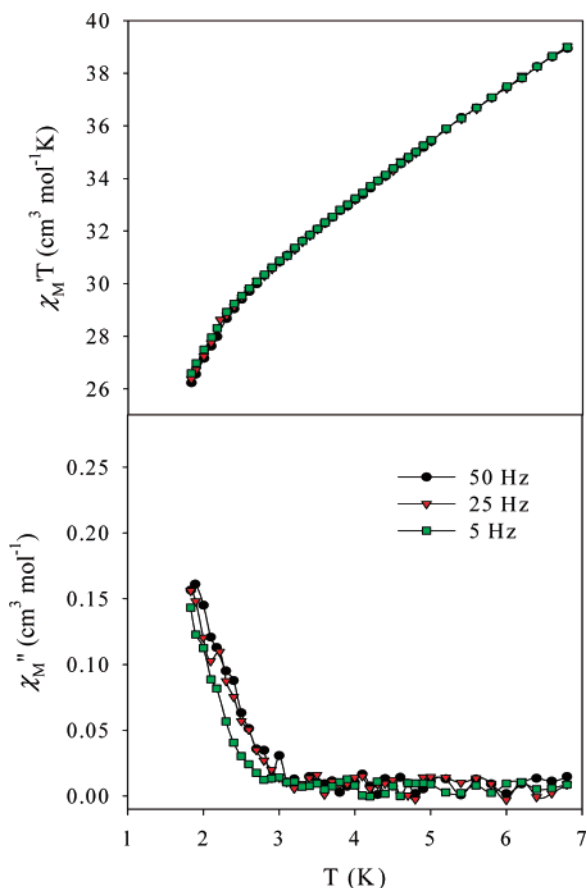
Figure 7. Plots of (top) the in-phase χ_M' (as $\chi_M'T$) vs T and (bottom) the out-of-phase χ_M'' AC susceptibility signals for complex **2**. The signals are noisy because of the small amounts of **2** available; the even-noisier signals at higher frequencies are not shown.

Figure 8. Plots of (top) the in-phase χ_M' (as $\chi_M'T$) vs T and (bottom) the out-of-phase χ_M'' AC susceptibility signals for complex **3**. The decrease in the χ_M'' signal in the 2−6 K range at 1000 Hz is an instrumentation artifact.

The AC susceptibility data for **2** are presented in Figure 7, which shows the in-phase AC susceptibility χ_M' (as $\chi_M'T$) versus T (Figure 7, top) and the out-of-phase ac susceptibility χ_M'' versus T (Figure 7, bottom) plots. In the absence of slow magnetization relaxation, that is, in the absence of an out-of-phase (χ_M'') signal, the in-phase susceptibility χ_M' is equal to the dc susceptibility χ_M. Thus, the in-phase χ_M' signal is a very useful way of determining the ground-state spin S of a molecule, particularly, when there are complications from low-lying excited states that interfere with determination of S from DC magnetization fits.[6e,g,29,30] Inspection of Figure 7 (top) shows a rapid, essentially linear decrease in $\chi_M'T$ with decreasing temperature, and this indicates depopulation of low-lying excited states with decreasing temperature, since occupation of only the ground state would give an essentially temperature-independent value. The strongly sloping plot attests to a particularly high density of low-lying excited states or ones with much larger S values than the ground state, and this rationalizes the failure to obtain good fits of the DC magnetization data assuming only the ground state is populated. Extrapolation of the $\chi_M'T$ signal to 0 K from above 3 K, to avoid the drop below 3 K caused by slow magnetization relaxation (vide infra), gives a value of ~24 cm^3 K mol^{-1} consistent with an $S = 7$ ground state and $g < 2$ (as expected for Mn). This is in agreement with the estimate from the DC magnetization fits above. In contrast, $S = 6$
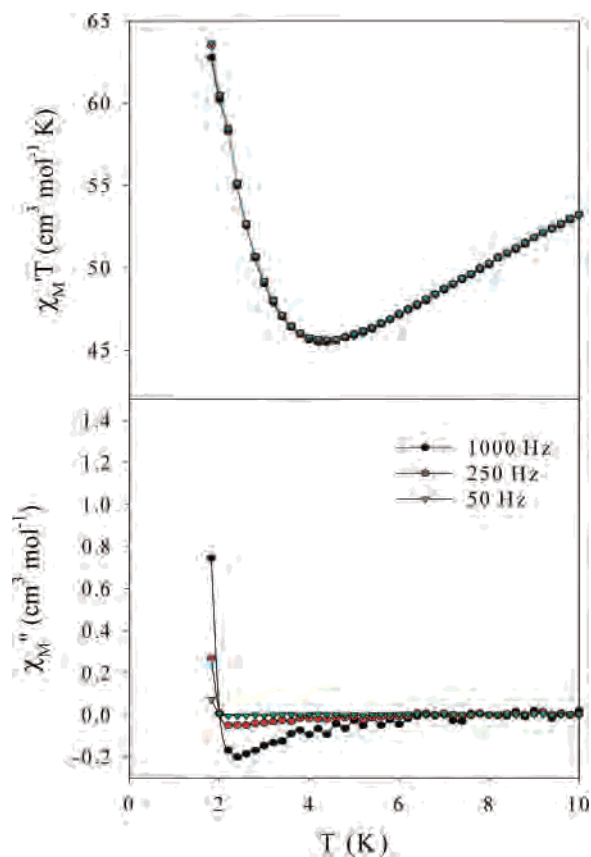
and 8 ground states would be expected to give values of less than 21 and 36 cm^3 K mol^{-1}, respectively.

Below 3 K, the $\chi_M'T$ shows the beginnings of a steeper and slightly frequency-dependent decrease, concomitant with the appearance of an out-of-phase AC susceptibility (χ_M'') signal (Figure 7, bottom). This is attributable to the onset of slow magnetization relaxation, suggesting that the $S = 7$ spin of **2·MeCN** and its negative magnetic anisotropy (negative D value) are resulting in it being an SMM. Since only weak tails are seen of χ_M'' signals whose peaks clearly lie far below the operating minimum of our SQUID susceptometer (1.8 K), it was necessary to study complex **2** at much lower temperatures to confirm whether it might be an SMM, and this was performed down to 0.04 K with a micro-SQUID apparatus (vide infra).

For complex **3**, the $\chi_M'T$ versus T plot (Figure 8, top) also shows a steep decrease with decreasing temperature, indicating the depopulation of low-lying excited states, as observed for **2**, but then below 4 K, it increases steeply. This behavior is attributed to the 1-D chain structure of this compound, and it indicates net parallel alignment along the chain of the overall spins of the repeating Mn_{22} units. Note that this statement is referring to the net alignment of the "giant spins" of adjacent Mn_{22} units as a result of the various interactions between the repeating units. Figure 4 suggests spin frustration effects are likely operative between the Mn_{22} units as a result of the triangular Mn_3 units in the bridging region, making a better rationalization of the net parallel "giant spin" align-

ments difficult. Below 2 K, there also appears a frequency-dependent χ_M'' signal (Figure 8, bottom) indicating slow magnetization relaxation, and this suggests that complex **3** might be the newest example of a single-chain magnet (SCM).[31] However, for this to be the case, studies to lower temperatures were necessary to confirm whether complex **3** really is a magnet or not. As for **2**, this was addressed by studies with a micro-SQUID down to 0.04 K.

Hysteresis Studies below 1.8 K. Hysteresis in magnetization versus applied DC field sweeps is the classical, diagnostic property of a magnet, including superparamagnets and SMMs below their blocking temperatures, T_B. Such studies were therefore performed down to 0.04 K on single crystals of **2·6MeCN·2CH₂Cl₂** and **3·7MeCN** using a micro-SQUID apparatus;[32] crystals were kept wet with mother liquor until mounted to prevent damage from solvent loss, and then covered with grease before transfer to the apparatus. The sensitivity and time resolution of a micro-SQUID magnetometer allow the study of very small single crystals in good contact with a thermal bath.

The resulting magnetization versus DC field responses are shown in Figure 9, which includes both a temperature dependence at a constant field sweep rate of 0.14 T s⁻¹ (Figure 9, top) and a field sweep rate dependence at a constant temperature of 0.04 K (Figure 9, bottom). Hysteresis loops were indeed observed below ∼1.2 K, whose coercivities increase with decreasing temperature and increasing field sweep rate, as expected for the superparamagnetic-like properties of a SMM below its blocking temperature (T_B). The data thus indicate complex **2·6MeCN·2CH₂Cl₂** to be a new addition to the family of SMMs. Clearly apparent in Figure 9 are steps in the hysteresis loops caused by quantum tunneling of magnetization (QTM) through the anisotropy barrier. Such steps at periodic values of applied field are a diagnostic signature of resonant QTM[33] and have been seen for several distinct classes of SMMs. In almost all cases, the first step in sweeping the field from one saturating value to the other occurs at zero field where the potential energy double-well is symmetric and M_s levels on one side of the barrier are degenerate (in resonance) with those on the other side, allowing tunneling to occur through the anisotropy barrier. The exception is when the first step is shifted away from zero field by the exchange-bias effect,[34] the weak interaction of a SMM with a neighboring SMM. The steps are thus positions of increased magnetization relaxation rate.
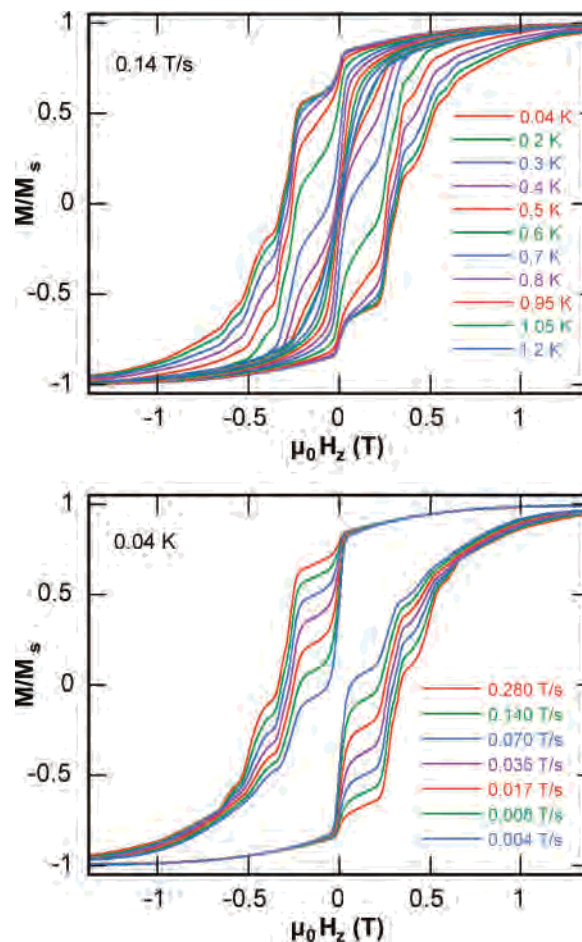

Figure 9. Magnetization (*M*) vs applied magnetic field (*H*) hysteresis loops for a single crystal of **2·6MeCN·2CH₂Cl₂**: (top) with a 0.14 T s⁻¹ sweep rate at the indicated temperatures and (bottom) at 0.04 K with the indicated field sweep rates. *M* is normalized to its saturation value, M_S.

It should be noted that the Mn₂₂ complex **2·6MeCN·2CH₂Cl₂** is the highest nuclearity complex to date to show resolved QTM steps in its hysteresis loops. This is in contrast to other such high nuclearity complexes where disorder of ligands, low-lying excited states, or disordered solvent molecules of crystallization in the vacancies between M_x molecules lead to a significant distribution of molecular environments and resulting broadening and smearing out of QTM steps in the hysteresis loops. Examples of the latter include Mn₁₈,[6g] Mn₂₁,[30] Mn₂₅,[29] Mn₂₆,[28] Mn₃₀,[6a,e] and Mn₈₄[6f] SMMs. In such cases, the presence of QTM is best confirmed by other methods, such as the detection of a temperature-independent relaxation rate at very low temperatures, magnetization decay with time,[6,28−30] and quantum hole digging.[6e,35,36] The steps in Figure 9 are clearly broadened, but not so much that they are no longer observable, showing that the distribution of molecular environments within the crystal or the broadening contribution of excited states are not so great for complex **2** compared with the other complexes mentioned above.

(31) (a) Clerac, R.; Miyasaka, H.; Yamashita, M.; Coulon, C. *J. Am. Chem. Soc.* **2002**, *124*, 12837. (b) Miyasaka, H.; Clerac, R.; Mizushima, K.; Sugiura, K.; Yamashita, M.; Wernsdorfer, W.; Coulon, C. *Inorg. Chem.* **2003**, *42*, 8203. (c) Caneschi, A.; Gatteschi, D.; Lalioti, N.; Sangregorio, C.; Sessoli, R.; Venturi, G.; Vindigni, A.; Rettori, A.; Pini, M. G.; Novak, M. A. *Europhys. Lett.* **2002**, *58*, 771. (d) Liu, T.-F.; Fu, d.; Gao, S.; Zhang, Y.-Z.; Sun, H.-L.; Su, G.; Liu, Y.-J. *J. Am. Chem. Soc.* **2003**, *125*, 13976. (e) Shaikh, N.; Panja, A.; Goswami, S.; Banerjee, P.; Vojtiek, P.; Zhang, Y.-Z.; Su, G.; Gao, S. *Inorg. Chem.* **2004**, *43*, 849. (f) Toma, l. M.; Lescouezec, R.; Lloret, F.; Julve, M.; Vaissermann, J.; Verdaguer, M. *Chem. Commun.* **2003**, *15*, 1850.
(32) Wernsdorfer, W. *Adv. Chem. Phys.* **2001**, *118*, 99.
(33) (a) Friedman, J. R.; Sarachik, M. P.; Tejada, J.; Ziolo, R. *Phys. Rev. Lett.* **1996**, *76*, 3830. (b) Thomas, L.; Lionti, L.; Ballou, R.; Gatteschi, D.; Sessoli, R.; Barbara, B. *Nature* **1996**, *383*, 145.
(34) Wernsdorfer, W.; Aliaga-Alcalde, N.; Hendrickson, D. N.; Christou, G. *Nature* **2002**, *416*, 406.

(35) Wernsdorfer, W.; Ohm, T.; Sangregorio, C.; Sessoli, R.; Mailly, D.; Paulsen, C. *Phys. Rev. Lett.* **1999**, *82*, 3903.
(36) Wernsdorfer, W.; Caneschi, A.; Sessoli, R.; Gatteschi, D.; Cornia, A.; Villar, V.; Paulsen, C. *Phys. Rev. Lett.* **2000**, *84*, 2965.
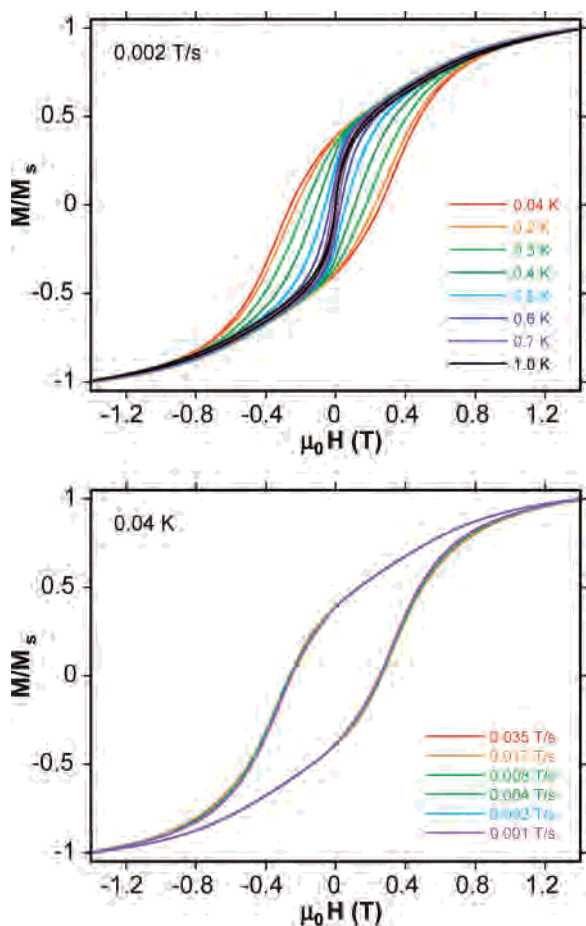
Figure 11. Arrhenius plots for (top) **2**·6MeCN·2CH$_2$Cl$_2$ and (bottom) **3**·7MeCN constructed from DC magnetization vs time decay data (see Supporting Information). The dashed lines are the fits of the thermally activated regions to the Arrhenius equation; see the text for the fit parameters.

Figure 10. Magnetization (*M*) vs applied magnetic field (*H*) hysteresis loops for a single crystal of **3**·7MeCN: (top) with a 0.002 T s^{-1} sweep rate at the indicated temperatures and (bottom) at 0.04 K with the indicated field sweep rates. *M* is normalized to its saturation value, M_S.

The appearance of well-resolved QTM steps in Figure 9 is beneficial in providing a direct determination of the *D* value of complex **2**. The field separation between steps, ΔH (in gauss) is proportional to *D* (in cm^{-1}) as given by eq 2, where the Bohr magneton μ_B is of value 4.6686×10^{-5} cm^{-1}

$$\Delta H = |D|/g\mu_B \qquad (2)$$

G^{-1} in these units. Measurement of the step positions in Figure 9 gave an average ΔH of ~0.27 T and thus a |*D*| value of ~0.25 cm^{-1} (0.36 K) assuming $g = 2.0$. Note that at such low temperatures there is not enough thermal energy to overcome the potential energy barrier, and essentially all magnetization relaxation is by QTM involving a two-phonon Orbach process via higher-lying M_s levels of the $S = 7$ ground state where the tunneling rates are faster. However, Figure 9 (top) shows that the hysteresis loops become essentially temperature-independent below ~0.2 K, indicating that only ground-state QTM from the lowest-lying $M_s = -7$ level to the $M_s = +7$ is occurring below this temperature.

For **3**·7MeCN, hysteresis loops are again observed below 1.0 K (Figure 10), but this time with no resolved QTM steps. In addition, there is still a distinct temperature dependence of the coercivity, which increases with decreasing temper-
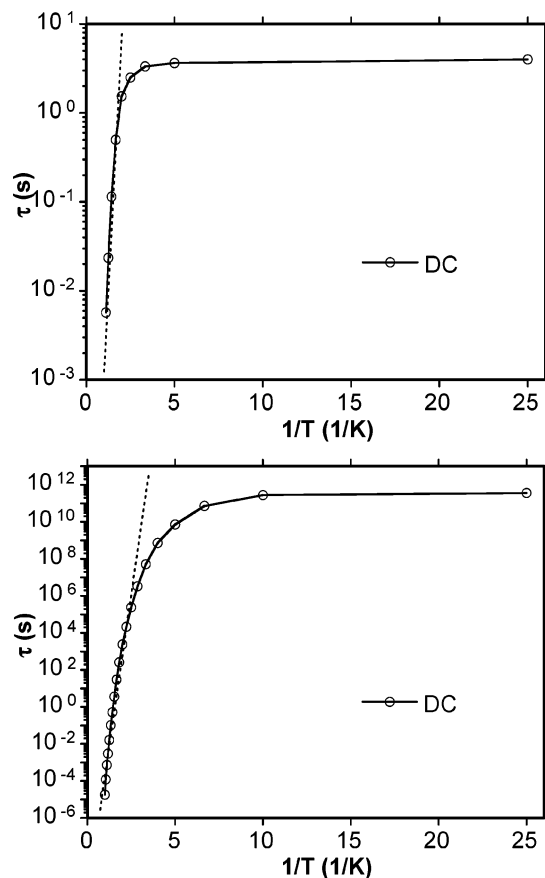
ature down to 0.04 K. However, there is only a very small scan rate dependence, which is not typical of a SMM. The overall behavior is thus consistent with a single-chain magnet with the barrier for the magnetization reversal arising from both the intrinsic barrier of each Mn$_{22}$ molecular unit, as seen for **2**, and an additional contribution from the intermolecular exchange interactions.[31b,37]

To characterize these systems further, magnetization versus time decay data were collected. The magnetization of the sample was first saturated in one direction with a large applied field at 5 K, the temperature decreased to a chosen value in the 0.04−1.0 K range, the applied field removed, and the magnetization of the sample monitored with time. The resulting data are shown in Figures S2 and S3 of Supporting Information for **2**·6MeCN·2CH$_2$Cl$_2$ and **3**·7MeCN, respectively. The decay data at each temperature were analyzed to give a set of relaxation time (τ) versus temperature data, which were used to construct the Arrhenius plots of Figure 11, based on the Arrhenius relationship of eq 3, where τ_0 is the pre-exponential factor, U_{eff} is the mean effective barrier to relaxation, and k is the Boltzmann constant. The fits of the thermally activated regions are

---

(37) Glauber, R. J. *J. Math. Phys.* **1963**, *4*, 294.

$$\tau = \tau_0 \exp(U_{\text{eff}}/kT) \qquad (3a)$$

$$\ln(\tau) = \ln(\tau_0) + U_{\text{eff}}/kT \qquad (3b)$$

shown as the dashed lines in Figure 12 and gave $U_{\text{eff}} = 6$ cm^{-1}, $\tau_0 = 9 \times 10^{-7}$ s for **2** and $U_{\text{eff}} = 11$ cm^{-1}, $\tau_0 = 4 \times 10^{-11}$ s for **3**. At the lowest temperatures, the relaxation time becomes temperature-independent, as expected for the relaxation only occurring via the ground state M_S levels. This temperature independence of the relaxation is a characteristic signature of QTM through the anisotropy barrier. Note also the distinct difference in τ_0 values between **2** and **3**: that for the former is typical for a SMM and the much smaller one for the latter is as expected for a nondiscrete system, in this case a 1-D polymer.

Single-chain magnetism is now well established with several well-documented examples.[31] It is well understood that both the intrinsic anisotropy of the repeating unit and the interunit exchange interactions will contribute to the overall barrier to magnetization relaxation. With the reasonable assumption that the intrinsic barrier of the Mn$_{22}$ unit is comparable in **2** and **3**, it is not surprising that the chain complex **3** should have the higher U_{eff}. Unfortunately, the data for **2** and **3** are not of sufficient quality to allow a full and precise analysis, but a rough estimate of the strength of the interaction between the Mn$_{22}$ units in **3** can still be obtained as follows: Since the upper limit to the relaxation barrier in a SCM is given by $(D + 4J)S^2$,[31] the first term arising from the molecular anisotropy and the second from the interaction (J) between repeating units, then the difference in U_{eff} between **3** and **2** can be equated with the $4JS^2$ term, leading to a value of $J \approx 0.03$ cm^{-1} ($\mathscr{H} = -2J\hat{S}_1\hat{S}_2$ convention). Such a weak value is consistent with the nature of the connection between the Mn$_{22}$ units in **3** and contributes to the overall small U_{eff}. In fact, the U_{eff} of 11 cm^{-1} for complex **3** is rather small compared with those of most other SCMs in the literature, which fall in the range of 50–154 K;[31] it is however comparable with the $U_{\text{eff}} = 9.9$ cm^{-1} found for [Mn$_7$O$_8$(O$_2$SePh)$_9$(H$_2$O)],[10] which also crystallizes as a chain structure. In any event, **3** is a SCM, and it contains the largest repeating unit of any SCM to date. It is important to note that the hysteresis loops are not caused by a three-dimensional ordering of the chains through interchain interactions. The temperature and sweep rate dependences of the hysteresis loops of **3·**7MeCN argue against a classical three-dimensional magnet. We should also add that any magnetic chain or other polymeric array with such large repeating units as found in **3** is very rare and comparable with the recently reported 3-D polymer of Mn$_{19}$ magnetic units.[38] Complexes **2** and **3** also provide an extremely rare example of a SMM, which has also been obtained in repeating form within a SCM.[39]

(38) Moushi, E. E.; Stamatatos, T. C.; Wernsdorfer, W.; Nastopoulos, V.; Christou, G.; Tasiopoulos, A. J. *Angew. Chem., Int. Ed.* **2006**, *45*, 7722.

(39) Miyasaka, H.; Nezu, T.; Sugimoto, K.; Sugiura, K.; Yamashita, M.; Clerac, R. *Chem.—Eur. J.* **2005**, *11*, 1592.

Conclusions

The use of phenylphosphinic acid (PhHPO$_2$H) in attempted ligand substitution reactions with [Mn$_{12}$O$_{12}$(O$_2$CEt)$_{16}$(H$_2$O)$_4$] has led instead to isolation of two related Mn$_{22}$ and [Mn$_{22}$]$_n$ products. These are structurally very similar and contain a core that is very different from that of the Mn$_{12}$ starting material. The compounds contain an oxidized form of the phenylphosphinate ligand employed, indicating the reaction to be extremely complicated. It is not possible to answer at the moment whether the Mn$_{12}$ core disruption is caused by the oxidized phenylphosphonate after it is formed or is concomitant with the ligand oxidation. Certainly given our successful previous isolation of Mn$_{12}$ compounds with diphenylphosphinate ligands, we do not believe it is merely a consequence of adding P-based ligands to the Mn$_{12}$ solution.

The Mn$_{22}$ structure is a new one, although it has recognizable Mn$_9$ subunits previously seen in discrete form. In addition, complex **2** has established a new record for how high a metal nuclearity an SMM can have and still show well resolved QTM steps. As stated earlier, it is extremely rare to see such steps for higher nuclearity complexes, for the various reasons mentioned. The overall relevance of this observation is that the crystal of **2** contains a relatively small distribution of environments (and thus of D values and relaxation barriers), otherwise the steps would be broadened and smeared out, and is thus a good candidate for any studies wishing to probe the physics of the QTM behavior of large molecules in more detail. While it was unfortunate that we could not discover a higher-yield route to this complex from the changes in the reaction conditions that we explored, the latter did at least have the beneficial result of providing a derivative of **2** that was a 1-D chain, namely, complex **3**. Once again, we see how at-first-glance trivial changes to a Mn reaction system, in this case a change in solvent from MeCN to MeCN/CH$_2$Cl$_2$, can have a profound effect upon the identity of the isolated product. Complex **3** also demonstrates magnetization hysteresis and thus is a new SCM, but steps are not observed for this compound, which is the usual case for SCMs. Finally, we note that **3** is the SCM with the largest repeating magnetic unit, and this suggests that there is no reason why a variety of other large SMMs, especially ones with large U_{eff}, such as [Mn$_{12}$O$_{12}$(O$_2$CR)$_{16}$(H$_2$O)$_4$], for example, could not be converted to SCMs with very high barriers by appropriate linkage with suitable bridging groups. These and other investigations are in progress.

Supporting Information Available: X-ray crystallographic data in CIF format for complexes **2·**6MeCN·2CH$_2$Cl$_2$ and **3·**7MeCN, plots of M/N_{μ_B} versus H/T for **2·**MeCN, and plots of magnetization versus time decay for **2** and **3**. This material is available free of charge via the Internet at http://pubs.acs.org.

IC7011292